



Vessel filtering and segmentation of coronary CT angiographic images

Yan Huang^{1,2} · Jinzhu Yang^{1,2} · Qi Sun^{1,2} · Shuang Ma^{1,2} · Yuliang Yuan^{1,2} · Wenjun Tan^{1,2} · Peng Cao^{1,2} · Chaolu Feng^{1,2}

Received: 1 October 2021 / Accepted: 22 April 2022 / Published online: 28 June 2022
© CARS 2022

Abstract

Purpose Coronary artery segmentation in coronary computed tomography angiography (CTA) images plays a crucial role in diagnosing cardiovascular diseases. However, due to the complexity of coronary CTA images and coronary structure, it is difficult to automatically segment coronary arteries accurately and efficiently from numerous coronary CTA images.

Method In this study, an automatic method based on symmetrical radiation filter (SRF) and D-means is presented. The SRF, which is applied to the three orthogonal planes, is designed to filter the suspicious vessel tissue according to the features of gradient changes on vascular boundaries to segment coronary arteries accurately and reduce computational cost. Additionally, the D-means local clustering is proposed to be embedded into vessel segmentation to eliminate noise impact in coronary CTA images.

Results The results of the proposed method were compared against the manual delineations in 210 coronary CTA data sets. The average values of true positive, false positive, Jaccard measure, and Dice coefficient were 0.9541 ± 0.0651 , 0.0812 ± 0.1024 , 0.8894 ± 0.1214 , and 0.9318 ± 0.0833 , respectively. Moreover, comparing the delineated data sets and public data sets showed that the proposed method is better than the related methods.

Conclusion The experimental results indicate that the proposed method can perform complete, robust, and accurate segmentation of coronary arteries with low computational cost. Therefore, the proposed method is proven effective in vessel segmentation of coronary CTA images without extensive training data and can meet clinical applications.

Keywords Coronary CTA · Vessel filtering · Vessel segmentation · Local clustering

Introduction

Coronary artery disease is the most common type of cardiovascular disease. If a coronary artery becomes narrowed or occluded due to plaque build-up, a decrease in blood flowing to the myocardium may cause ischemia, leading to fatal consequences [1]. In recent years, coronary computed tomography angiography (CTA) images have become critical for cardiovascular disease filtering, diagnosis, and treatment. However, it is difficult and time-consuming for clinicians to track and analyze coronary arteries manually. Therefore, the accurate and automatic segmentation of coronary arter-

ies in CTA images has an important practical significance and clinical value [2]. The state-of-the-art methods for the segmentation of coronary arteries can be divided into the following categories [3,4].

Models that correspond to the prior assumption are applied to the target vessels, such as a vascular model, a geometric model, a hybrid model, and a specific model. Boskamp et al. [5] designed a series of procedures to segment vessels according to vessel intensity distributions and morphology features, but it is sensitive to the noise of the image. To address those problems, many scholars proposed geometric models to detect vessel boundaries. Huang et al. [6] designed a method for accurate vessel segmentation based on the cylinder model. Although the geometric model can naturally deal with topological structure changes, it is low efficient and sensitive to noise. Therefore, various hybrid models have been proposed to segment vessels. A hybrid model-based method was proposed to simulate the generation of the vascular tree by using constraint construction optimization and flow-

✉ Jinzhu Yang
yangjinzhu@cse.neu.edu.cn

¹ Key Laboratory of Intelligent Computing in Medical Image, Ministry of Education, Northeastern University, Shenyang, Liaoning, China

² School of Computer Science and Engineering, Northeastern University, Shenyang, Liaoning, China

related geometric constraints [7]. Except for normal vessels, vessel bifurcations and abnormal vessels will increase the difficulties of vessel segmentation. Thus, a specific vascular model was designed for specific vascular shapes [8].

Features based on vessel measures estimate the models in CTA images, which can be image features, structural features, and feature transformations. An intensity-based multi-level classification model was proposed to extract features. Zhuang et al. [9] proposed an improved super-pixel generation algorithm that incorporates both gray-level and luminosity-based information to improve simple linear iterative clustering algorithms. A popular method in detecting vessels is to use the second-derivative information to characterize the geometric shape of local images, such as Hessian matrix transformation (HMT) [10]. Ge et al. [11] proposed a two-step segmentation algorithm based on Hessian matrix and level set using Hessian matrix eigenvalues, feature vectors, and evolution of a level set function.

Either the model-based or feature-based methods require a suitable vascular segmentation scheme to achieve good segmentation results. Generally, a strategy of vascular segmentation is: first, pre-processing or pre-segmenting target images [12]; second, using a region-growing based method, an active contour model method, and a centerline tracking-based method to extract vessels and obtain the boundaries [13,14]; finally, adopting a post-processing strategy to extract complete target vessels [3]. Du et al. [15] proposed a new segmentation framework for 3D coronary artery trees by integrating noise reduction, candidate region detection, geometric feature extraction, and coronary artery tracking techniques.

A deep learning-based method has been widely used in vascular segmentation in recent years. In contrast to traditional methods, it does not need to design models, features, or segmentation schemes [4,16]. Gu et al. [17] proposed a global feature embedded network (GFE-Net) for coronary arteries segmentation in CTA images. The GFE-Net improves V-Net uses a noisy activating function to suppress CTA image noise during the network down-sampling process. Shen et al. [18] proposed a 3D fully convolutional network (FCN) integrating an attention gate for coarse segmentation of coronary arteries. The coarse segmentation is then optimized using the level set function to obtain a refined, smooth segmentation. Although the deep learning-based method has made some achievements in vascular segmentation, its application in vascular segmentation of coronary CTA images still presents great challenges [19,20].

In this paper, we propose an automatic method for coronary artery segmentation. The main contributions are summarized as follows:

1. We design a two-dimensional (2D) symmetrical radiation filter (SRF) which is applied to the tissue on three orthogonal planes (the axial, coronal, and sagittal planes) rather than a cross-sectional plane.
2. We propose a D-means local clustering segmentation scheme that performs iterative local calculations on vascular tissue to avoid the influence of cardiac motion artifacts and unsteadiness of the contrast agent concentration.
3. The proposed method has low complexity, low computational cost, a broad clinical application, and a low hardware requirement, which can fully meet the need of clinicians.

Method

The framework of the leading segmentation procedures is depicted in Fig. 1. The proposed method has two new algorithms: the SRF used to filter the suspicious vessel regions and the D-means local clustering used to eliminate the impact of noise in coronary CTA images. Firstly, we describe the SRF-based vessel filtering method in “Vessel filtering” section, including the theory and application. Then, we describe the vessel segmentation method in “Vessel segmentation” section, including the use of SRF and D-means local clustering.

Vessel filtering

Theory of SRF

SRF is a vessel filter used to remove non-vessel tissue by calculating an intensity value of symmetrical vascular gradient and judging whether it meets a filtering threshold of gradient symmetry of vessels. Figure 2 depicts the SRF method.

Suppose that a point x_0 in a vessel on a 2D plane emits ray pairs to the surroundings in a range of maximum distance D_{\max} and π angles. The ray pairs $\pm u(\alpha)$ are two rays emitted from a point x_0 in opposite directions. As well known, in coronary CTA images, vessels are brighter than the surrounding structures. The maximum gradient value will be at the inner and outer vessel boundary. Therefore, the vessel boundary should be detected first. $b(x)$ denotes a boundary measure with a sign along a ray $u(\alpha)$ at a point x , defined as follows:

$$b(x) = (|\nabla_{\sigma} I(x)|) \text{sign}(\nabla_{\sigma} I(x)) \quad (1)$$

where $I(x)$ denotes one-dimensional intensity distribution, and $\nabla_{\sigma} I(x)$ denotes a gradient of the point x . σ denotes a spatial scale of the vessel boundary determined according to a thickness of a vessel wall, set to 1.5mm. Considering the direction of the gradient, $\text{sign}(\nabla_{\sigma} I(x))$ is used to distinguish whether the change of vascular boundary is rising (from dark

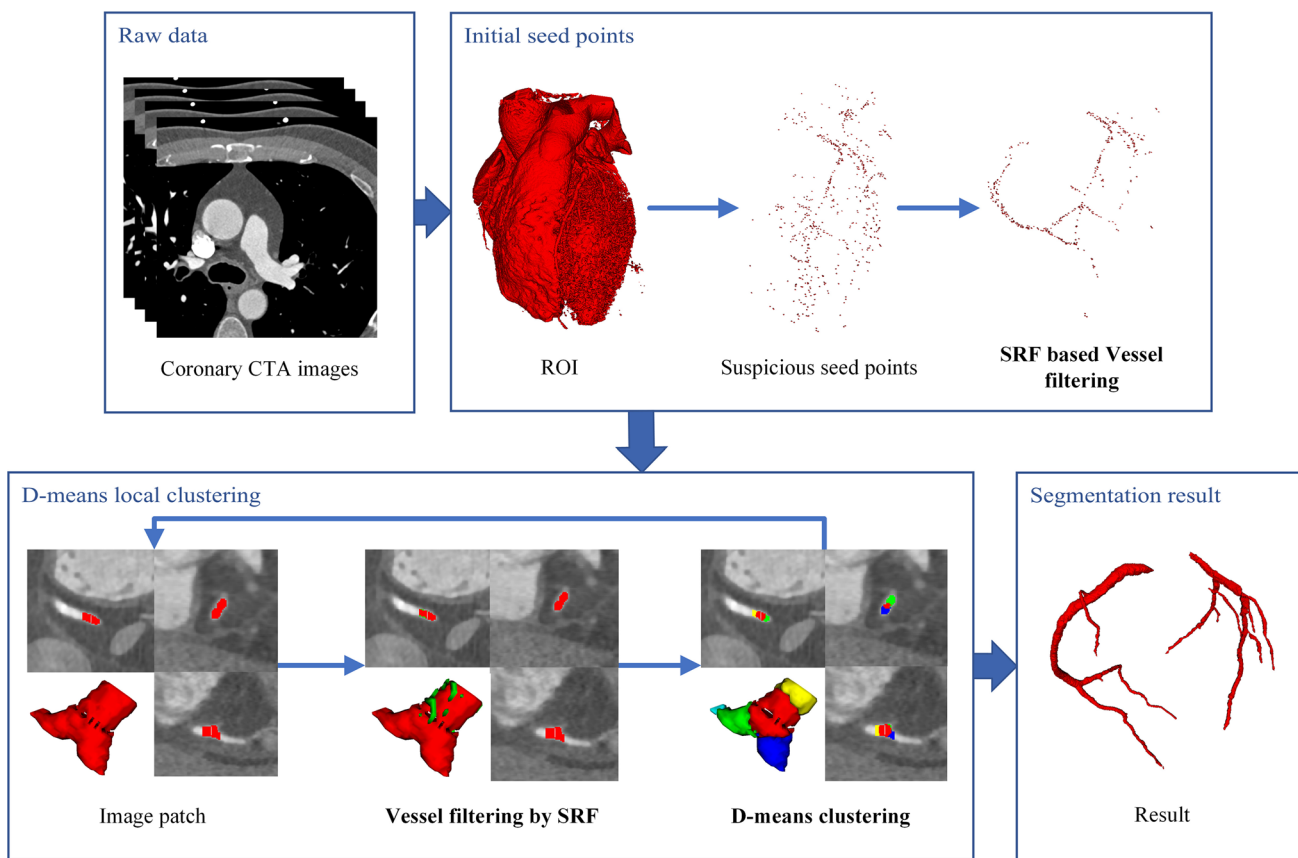


Fig. 1 Framework of vessel filtering and segmentation of coronary CTA images. In the D-means local clustering stage, each step is composed of four views: axial view on the top left, sagittal view on the top right, VR view on the bottom left, and coronal view on the bottom right. At

the image patch step, the non-coronary artery tissue marked in green is removed by the SRF; at the D-means clustering step, multicolored tissue is used to display the D-means clustering results

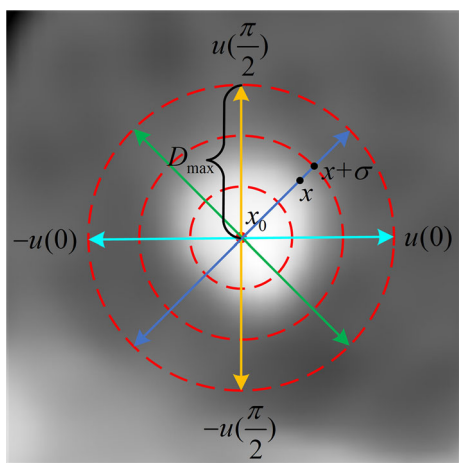


Fig. 2 Diagram of SRF. Each colored line with a double-headed arrow represents a pair of rays. Each red dotted circle represents the distance traveled by the rays

to dark. Points inside the vessel are surrounded by falling boundaries except for two conditions: One is points outside the vessels are surrounded by bright tissue-like vessels and ventricles; the other is points belong to abnormal substances like calcified plaques and metal stents.

Since SRF is designed based on the gradient symmetry of vessels, the maximum falling edge response $E(x_0, u(\alpha))$ should be searched at the different locations x in a step size of 0.6mm along the ray $u(\alpha)$ within the maximum distance D_{max} . The step size is set according to the vessel diameter and the average physical size of coronary CTA images. The definition of function $E(x_0, u(\alpha))$ is given by:

$$E(x_0, u(\alpha)) = \max_{x \in [x_0, x_0 + D_{max}u(\alpha)]} \{-b(x), 0\} \tag{2}$$

where $u(\alpha) = \sin(\alpha)u_1 + \cos(\alpha)u_2$, and u_1 and u_2 are two directions of the 2D plane. $\alpha, \alpha \in [0, \pi)$, denotes an angle of the ray. The maximum distance D_{max} is set to 8mm, which only needs to exceed the maximum vessel diameter according to the vascular physiology structure. For the ray

to bright) or falling (from bright to dark) [12]. The change from the inner to the outer vessel must present from bright

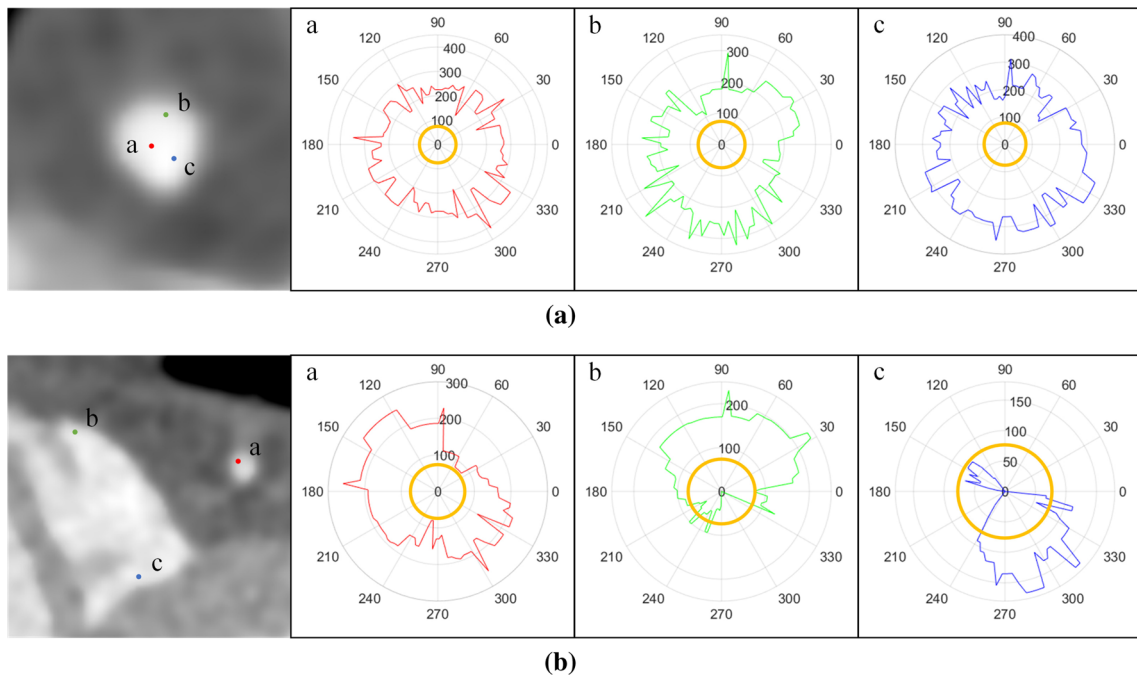


Fig. 3 Polar coordinates used to illustrate the SRF. **a** The polar coordinates for any three points a, b, and c in the vessel used to illustrate the SRF. **b** The polar coordinates for point a in the vessel and points b, c in the right ventricle used to illustrate the SRF. The first column

shows local axial planes of coronary CTA images. The red, green, and blue curves represent the maximum falling edge responses of a, b, and c points in each direction, respectively. The yellow circle represents the minimum threshold of the maximum falling edge responses

pairs $\pm u(\alpha)$, there are two maximum falling edge responses $E(x_0, u(\alpha))$ and $E(x_0, -u(\alpha))$. When the two maximum falling edge responses both satisfy conditions, the ray pairs have gradient symmetry. Thus, the gradient symmetry function $B(x_0, \pm u(\alpha))$ is given by:

$$B(x_0, \pm u(\alpha)) = P(E(x_0, u(\alpha)) > T_1 \wedge E(x_0, -u(\alpha)) > T_1) \tag{3}$$

where T_1 denotes a minimum threshold of the maximum falling edge responses, set to 70. The binary function P is equal to 1 when the expression condition inside the function is evaluated to be satisfied. Otherwise, it is equal to 0.

On a 2D plane, there are N ray pairs, set to 20 according to the size of coronary arteries and CTA images. Thus, the definition of the SRF function is given by:

$$F(x_0) = P\left(\left(\frac{1}{N} \sum_{i=0}^{N-1} B\left(x_0, \pm u\left(\frac{\pi i}{N}\right)\right)\right) > T_2\right) \tag{4}$$

where T_2 denotes a minimum threshold of a proportion of ray pairs that satisfy the gradient symmetry, set to 0.65. When the proportion of the ray pairs emitted from the point x_0 to satisfy the gradient symmetry function $B(x_0, \pm u(\frac{\pi i}{N}))$ is greater than the threshold T_2 , the point x_0 belongs to the vessels. The fixed parameters related to SRF are obtained by

statistical methods, such as receiver operating characteristic (ROC) curves and histogram analysis.

SRF is designed according to the feature of the descending boundary from the inner to the outer vessel on the 2D plane. Unlike the filter designed in the literature [12], SRF does not require the calculated point to be the center point of the vessel. As shown in Fig. 3a, as long as the points (like points a, b, and c) are in the vessel, their gradient of SRF is similar, and all have symmetry features of gradient change. Nevertheless, if the points are not in the vessel, they will not be similar and not have the symmetry feature like points b and c depicted in Fig. 3b.

Application of SRF

Compared with the state-of-the-art 3D vessel filter [21,22], SRF is a 2D vessel filter designed based on the gradient symmetry of vessels on a 2D oblique plane, which is used to reduce the computational cost for clinical application. Generally, a 2D vessel filter is applied to a cross-sectional plane obtained based on the HMT, like the method used in the literature [12]. HMT is time-consuming and often inaccurate for weak vessels [21,22]. As we can observe from Fig. 4, whether in vascular or non-vascular cross-sectional planes, points have strong gradient symmetry (the first column of Fig. 4a and c). Even using multi-scales, the HMT has a deviation

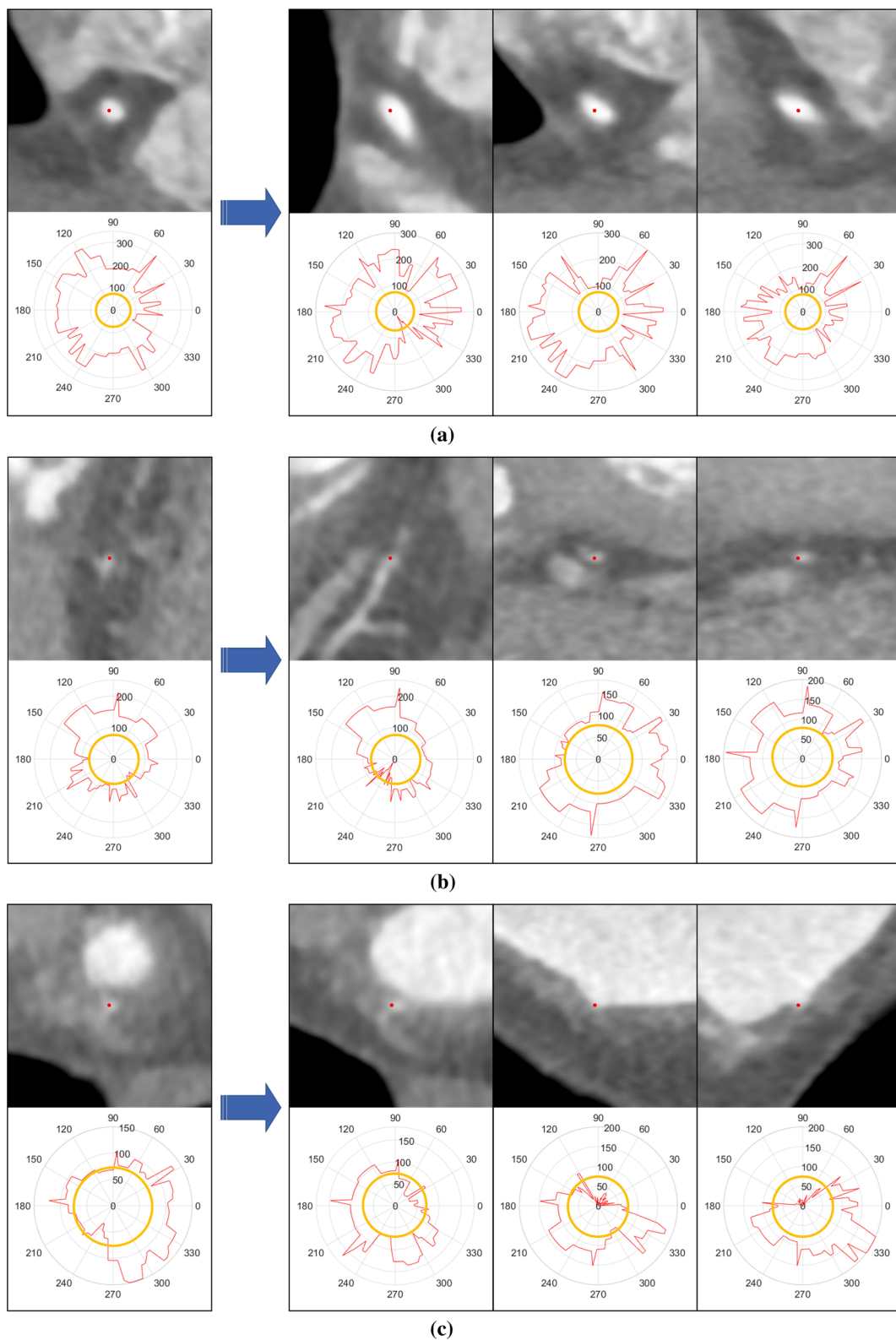


Fig. 4 2D planes and polar coordinates used to illustrate the SRF. The first column depicts the cross-sectional planes of the points obtained based on HMT and their corresponding polar coordinates. The second to the fourth columns depict the axial, coronal, and sagittal planes of the points and their corresponding polar coordinates. The red curve repre-

sents the maximum falling edge responses of the red point. The yellow circle represents the minimum threshold of the maximum falling edge responses. The points in **a** and **b** are in vessels. The point in **c** is not in the vessel

(the first column of Fig. 4b). However, the three orthogonal planes can effectively distinguish inside points (the second to fourth columns of Fig. 4a and b) from the outside points (the second to the fourth columns of Fig. 4c).

Taking the feature of SRF and coronary CTA images into account, we integrated SRF values from three orthogonal planes (axial, coronal, and sagittal planes) into one judgment to replace a judgment of SRF values from one cross-sectional plane. When two or more 2D orthogonal planes meet the intensity value, the point is considered to satisfy the gradient symmetry and belongs to vessels.

Vessel segmentation

In this paper, we integrate the designed SRF-based vessel filtering and D-means local clustering into coronary artery segmentation (as depicted in Fig. 1). Firstly, the initial seed points are obtained by state-of-the-art algorithms with the SRF to further ensure the initial seed points are effective for subsequent iterations of vessel segmentation. Secondly, the D-means local clustering is integrated into the iterative process to obtain image patches used to update vessel segmentation parameters. During each iteration, the SRF is used again to ensure that the image patches belong to the coronary arteries. Finally, the vessel segmentation is done when all the initial seed points and image patches are completed.

Initial seed points

The initial seed points that are generally starting points for region segmentation can be obtained in many ways, such as the methods described in the literature [10,23,24]. The initial seed points are coarse in this paper, i.e., only at least two effective seed points in each main coronary tree are enough, and numerous seed points and false seed points are tolerated. Therefore, to reduce the computational cost, two coarse thresholds, set to 130 Hounsfield units (HU) and 500 HU, are firstly used to extract a region of interest (ROI) for the initial seed points. Secondly, a Hessian matrix with a single scale determined by the average radius of coronary arteries and a tubular structure similarity function is adopted to get suspicious seed points with robust tubular structure features. Finally, the effective seed points are obtained by SRF.

D-means local clustering

Vessels in CT images appear unstable changes such as large changes in CT values, dislocation of coronary arteries, and blurry artifacts in coronary CTA images. Only in a small range of regions, the features are similar. Thus, the D-means local clustering algorithm is critical in the iterative segmentation process. It can divide a large region into multiple localized small image patches so that these small image

patches can update the parameters required for the next iteration segmentation.

There are many state-of-the-art clustering algorithms such as K-means [25], K-medoids [26], density-based spatial clustering of applications with noise (DBSCAN) [27], and hierarchical clustering [28]. The D-means local clustering is the evolution of K-means and DBSCAN, which makes the distance between all target points in the clustering domain and the clustering center meet the defined conditions. Moreover, there is no need to specify the number of clusters before clustering.

Let us assume a data set X composed of m voxels from a region V . The process of the D-means clustering algorithm is to divide the data set X into N clusters C_i according to a distance D as defined in the following equation:

$$X = \left\{ x_{ij} \mid \begin{matrix} x_{ij} \\ i \in [1, N], j \in [1, |C_i|] \end{matrix} \in V \right\} \quad (5)$$

where x_{ij} is a voxel of the region V . D is set 4mm according to the maximum radius of the coronary artery. Each cluster C_i has a cluster center μ_i defined as follows:

$$\mu_i = \frac{1}{|C_i|} \sum_{j \in [1, |C_i|]} x_{ij} \quad (6)$$

where C_i is defined as:

$$C_i = \{ (x_{ij}, \mu_i) \mid d(x_{ij}, \mu_i) \leq D \} \quad (7)$$

the distance $d(x_{ij}, \mu_i)$ is defined as follows:

$$d(x_{ij}, \mu_i) = \sum_{x_{ij} \in C_i} \|x_{ij} - \mu_i\| \quad (8)$$

By selecting Euclidean distance as the criterion of similarity and distance, the number of clusters N whose distance d from each point x_{ij} to the cluster center μ_i is less than or equal to D is calculated. Figure 5 depicts the process of dividing a dataset X into three predefined clusters.

Segmentation procedures

Vessel segmentation is an iterative process. During the iterative process, the image patches are grown coarsely by two thresholds Thre_{low} and $\text{Thre}_{\text{high}}$. Thre_{low} and $\text{Thre}_{\text{high}}$ denote a low CT value threshold and a high CT value threshold, respectively. They are constantly updated during the growth

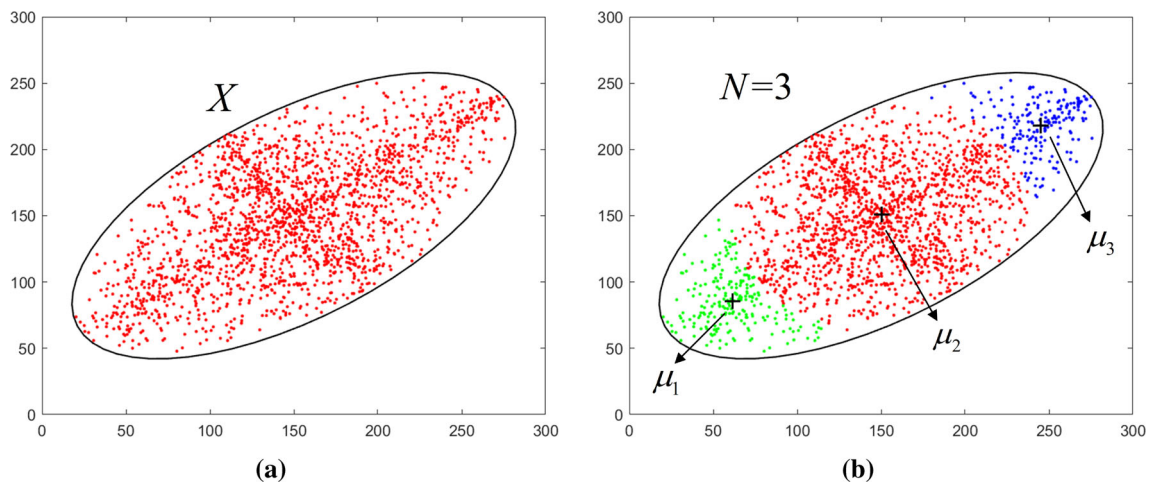


Fig. 5 Schematic diagram of D-means clustering. The red points in **a** are the set X of points to be clustered. **b** is the three clusters (green points, red points, and blue points) obtained after D-means local clustering on **a**. The crosshair in each cluster represents their corresponding cluster center points

of each image patches, which are defined by CT mean $Mean_{CT}$ and standard deviation SD_{CT} as follows:

$$\begin{cases} Thre_{low} = Mean_{CT} - SD_{CT} \\ Thre_{high} = Mean_{CT} + SD_{CT} \end{cases} \quad (9)$$

where $Mean_{CT}$ and SD_{CT} denote CT value mean and standard deviation, respectively. They are calculated by the last image patches. For the first image patch, they are calculated by the 26 neighborhoods of the initial seed points. The image patch IP is defined as follows:

$$IP = \{x_{CT} \mid x_{CT} \geq Thre_{low} \wedge x_{CT} \leq Thre_{high}\}. \quad (10)$$

where x_{CT} denotes the CT value at x . The image patch IP will contain many false points which need to be removed. Thus, the SRF is applied to ensure that the reserved image patch RIP given by (11) is coronary arteries (see the ‘‘Vessel filtering’’ section).

$$RIP = \{x \mid x \in IP \wedge x \in SRFV\} \quad (11)$$

where SRFV denotes a set of points that satisfies the condition of SRF. As described in ‘‘D-means local clustering’’ section, the image patch RIP should be clustered to ensure that the two thresholds $Thre_{low}$ and $Thre_{high}$ used for the next iterative segmentation are accurate. Thus, the D-means local clustering algorithm is used to get the regional cluster sets C_N :

$$C_N = \left\{ C_i \mid C_i \subseteq RIP \right\}_{i \in [1, N]} \quad (12)$$

The cluster C_i is the input image patch for the next iteration. When all seed points and image patches are completed, the segmentation is done.

Results

Materials

The proposed method was implemented in Visual Studio software (C/C++) and MATLAB software and executed on a desktop computer equipped with an Intel(R) Core (TM) i5-4590 HQ processor (3.30 GHz) and 16 GB of RAM.

Since there are no public data sets used for testing and verification in coronary artery segmentation, we randomly collected a total of 210 data sets of coronary CTA images from different manufacturers (GE, Philips, and Siemens), different equipment, and different hospitals. The average voxel size of images is $512 \times 512 \times 291$ with an average physical size of $0.40 \text{ mm} \times 0.40 \text{ mm} \times 0.47 \text{ mm}$. There are 120 healthy data sets and 90 diseased data sets, of which 50 are significant stenosis ($\geq 50\%$ luminal narrowing).

The manual delineation is time-consuming and energy-consuming because of the complex coronary artery structure, inconsistent image quality, and different expert requirements for coronary artery segmentation. Therefore, three senior cardiovascular experts have manually delineated the data based on the results of the proposed method by adding the missing coronary arteries and removing non-coronary arteries.

Evaluation metrics

The results were compared with those manually delineated by experts to evaluate the accuracy of the segmentation results.

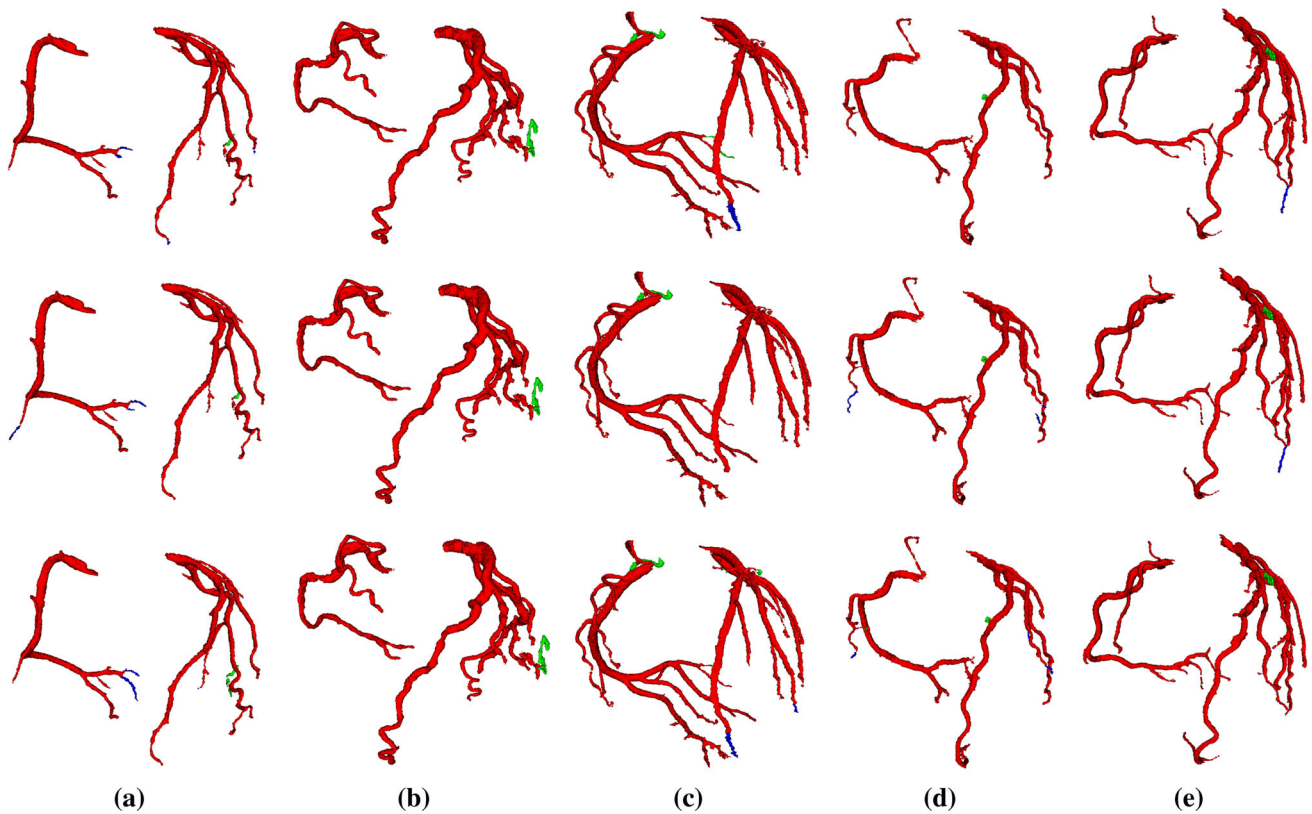


Fig. 6 Examples of VR images of coronary artery segmentation results **a, b**. Red and green regions are the segmentation results of the proposed method, and especially green regions are the non-coronary artery tissue removed by experts. Blue regions are missing coronary artery

tissue added by experts. Each row compares the segmented results of the proposed method and the manual delineations of experts 1, 2, and 3, respectively

Four metrics are used to evaluate the performance of the coronary artery segmentation methods: true positive (13), false positive (14), Jaccard measure (15), Dice coefficient (16):

$$TP = \frac{|S_{\text{auto}} \cap S_{\text{label}}|}{|S_{\text{label}}|} \quad (13)$$

$$FP = \frac{|S_{\text{auto}}| - |S_{\text{auto}} \cap S_{\text{label}}|}{|S_{\text{label}}|} \quad (14)$$

$$JM = \frac{|S_{\text{auto}} \cap S_{\text{label}}|}{|S_{\text{auto}} \cup S_{\text{label}}|} \quad (15)$$

$$DC = \frac{2 \times |S_{\text{auto}} \cap S_{\text{label}}|}{|S_{\text{auto}}| + |S_{\text{label}}|} \quad (16)$$

where S_{auto} and S_{label} denote the coronary artery region obtained by automatic segmentation and manual delineation, respectively.

Performance

The examples of the segmentation results and corresponding manual delineations are shown in Fig. 6. We can observe from Fig. 6 that the segmented results in this paper are highly consistent with the tissue manually delineated by three experts. For some undersegmented tissue, the manual delineations vary considerably.

Figure 7 shows box plots of the four metrics obtained after quantitative evaluation of the segmented results and the results manually delineated by experts. We can observe from Fig. 7 that the results obtained by the proposed method are consistent with the results manually delineated by experts. Compared with the three experts, the mean medians of TP, FP, JM, and DC are 0.9837, 0.0258, 0.9558, and 0.9875, respectively.

We also evaluated the segmented results of diseased data and healthy data in the data sets separately. The mean value and standard deviation of four metrics are shown in Table 1. From Table 1, we can observe that the proposed method has good performance on the healthy data sets as well as the diseased data sets.

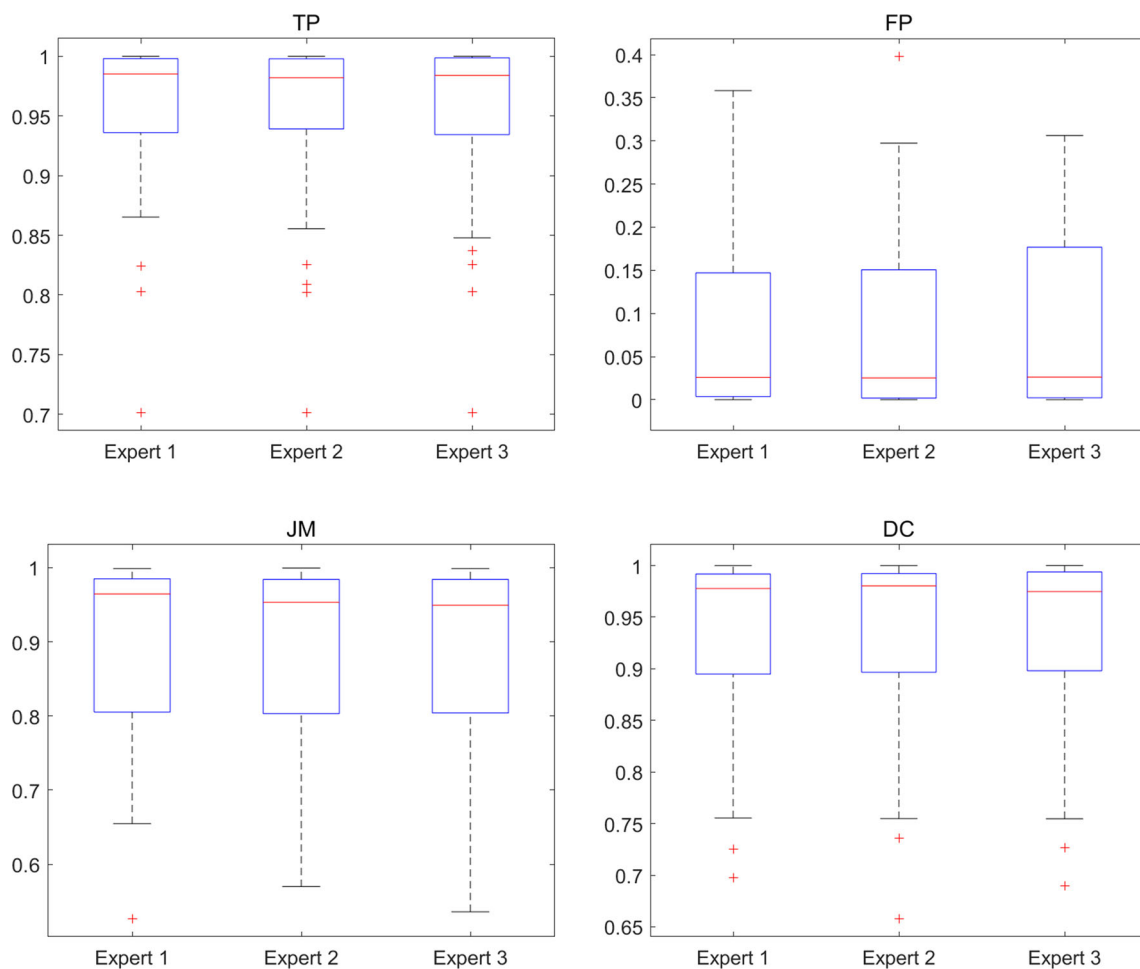


Fig. 7 Box plots of four metrics of the segmentation results

Table 1 Performance of the proposed method compared with the manual delineations on diseased data sets and healthy data sets, respectively

Metrics	Manual delin. 1		Manual delin. 2		Manual delin. 3	
	Diseased	Healthy	Diseased	Healthy	Diseased	Healthy
TP	0.9283 ± 0.0810	0.9765 ± 0.0357	0.9274 ± 0.0850	0.9728 ± 0.0391	0.9278 ± 0.0826	0.9729 ± 0.0407
FP	0.0906 ± 0.1165	0.0708 ± 0.0858	0.0902 ± 0.1237	0.0744 ± 0.0912	0.0909 ± 0.1170	0.0771 ± 0.0919
JM	0.8643 ± 0.1377	0.9130 ± 0.1025	0.8629 ± 0.1374	0.9099 ± 0.1034	0.8601 ± 0.1420	0.9067 ± 0.1070
DC	0.9079 ± 0.0987	0.9512 ± 0.0621	0.9053 ± 0.1020	0.9515 ± 0.0634	0.9070 ± 0.0985	0.9500 ± 0.0660

1. Manual delin 1, 2, and 3 represent the modification done by expert 1, 2, and 3, respectively, 2. All data are presented in the form of mean \pm standard deviation

To illustrate the segmentation error of the proposed method, we compared the error between each of the manual delineations. The mean value and standard deviation of four metrics were calculated between the manual delineation results of two experts in Table 2. Table 3 shows the mean value and standard deviation of four metrics of our proposed method compared with the manual delineation results. From the results, we can observe that the error between each of the manual delineations is close to the results of the proposed method.

Although there are no public gold standard data sets for evaluating coronary artery segmentation, the 3D Cardiovascular Imaging: a MICCAI (Medical Image Computing and Computer-Assisted Intervention) segmentation challenge workshop held in 2012 provides a framework for stenosis detection and evaluation. This evaluation framework provides 48 sets of CTA images, including 18 training sets and 30 test sets. 26% and 32% of the lesions are significant ($\geq 50\%$ luminal narrowing) for training and test datasets, respectively [29]. The evaluation method uses the common

Table 2 The measurement values of the four metrics obtained by comparing each of the manual delineation results

Metrics	Exp1 vs Exp2	Exp1 vs Exp3	Exp2 vs Exp3	Average
TP	0.9700 ± 0.0587	0.9689 ± 0.0612	0.9712 ± 0.0560	0.9700 ± 0.0586
FP	0.0538 ± 0.0614	0.0579 ± 0.0599	0.0510 ± 0.0624	0.0542 ± 0.0612
JM	0.9120 ± 0.1077	0.9096 ± 0.1020	0.9126 ± 0.0980	0.9114 ± 0.1026
DC	0.9645 ± 0.0719	0.9612 ± 0.0840	0.9688 ± 0.0712	0.9648 ± 0.0757

1. Exp stands for Expert 1, 2, and 3 represent different experts, respectively, 2. All data are presented in the form of mean ± standard deviation

Table 3 The measurement values of the four metrics obtained by comparing between the proposed method and the manual delineation results

Metrics	Manual delin. 1	Manual delin. 2	Manual delin. 3	Average
TP	0.9557 ± 0.0636	0.9532 ± 0.0663	0.9534 ± 0.0655	0.9541 ± 0.0651
FP	0.0794 ± 0.0995	0.0812 ± 0.1054	0.0830 ± 0.1024	0.0812 ± 0.1024
JM	0.8920 ± 0.1298	0.8896 ± 0.1200	0.8866 ± 0.1240	0.8894 ± 0.1214
DC	0.9325 ± 0.0819	0.9315 ± 0.0845	0.9314 ± 0.0834	0.9318 ± 0.0833

1. Manual delin 1, 2, and 3 represent the modification done by expert 1, 2, and 3, respectively 2. All data are presented in the form of mean ± standard deviation

delineation of three observers as the gold standard. Since the framework has been closed, we can only evaluate 18 training sets with the ground truth. The experimental results are shown in Table 4.

As deep learning has been widely used in segmentation and has achieved significant results, the proposed method was also compared with deep learning-based methods [17, 18]. The architectures are described in the fifth paragraph of the introduction section. According to the literature [17], the learning rate, optimizer, and number of epochs are 1×10^{-4} , Adam, and 200, respectively. According to the literature [18], the learning rate, optimizer, and number of epochs are 1×10^{-5} , Adam, and 500, respectively. The common manual delineations are used as ground truth to test 210 data sets. According to the general requirements of deep learning, 147 data sets were selected as the training sets, while 32 data sets were selected as the validation sets, and the others were used as the test sets. The experimental results are shown in Table 5.

The computational cost of the critical processes of the proposed method besides the HMT method was carried out on the 210 data sets (see Table 6). The most time-consuming procedure is obtaining the initial seed point, which accounts for 62.89% of the total time, whereas the SRF and local clustering segmentation account for 13.80% and 15.91%, respectively. The execution time using the HMT to acquire cross-sectional planes is 5.27 times the total computational cost of the proposed method, which is indicated in the last column of Table 6.

Discussion

The proposed method has been tested on 210 randomly obtained data sets, and the results are promising. We can

observe from Fig. 6 that the results are consistent with the manual delineations, which can fully include the left and right coronary arteries as well as branches. Although there may be local oversegmentation, they do not affect the overall structure of the coronary arteries. There may also be local undersegmentation mainly focused on the end of coronary arteries, but the manual delineations also have some disputes. As we can observe from the box plots of four metrics of segmentation results depicted in Fig. 7, the segmentation results have good clustering properties. The mean median of *TP* is 0.9837, which indicates that the results are relatively complete with less undersegmentation. The mean median of *FP* is 0.0258, which indicates that the error of oversegmentation is also within a small range.

To prove the segmentation error and clinical application, we conducted a comparative experiment, which results means that the proposed method is very close to the error of the manual delineations (see Table 2 and Table 3) and can fully meet clinical use. Furthermore, the proposed method was also tested and evaluated on the diseased and healthy data sets, respectively. The experimental results (see Table 1 and Table 4) are close to the results of the three observers, which means the proposed method has good adaptability to diseased data and can not be interfered with various factors such as calcified plaques, lipid plaques, hybrid plaques, and stents. For the healthy data, the segmented results are better than the diseased data, but there are still some poor segmented results. Although the healthy data are not affected by lesions, they are still easily affected by other factors, such as machine artifacts, motion artifacts, and unsteadiness of the contrast agent concentration, which result in poor image quality and seriously affect the segmented results.

We also compared our results with the related methods based on deep learning found in the literature. The exper-

Table 4 Performance of the proposed method compared with related methods on public data sets

Method	Dice % Diseased	Dice % Healthy	MSD mm Diseased	MSD mm Healthy	MaxD mm Diseased	MaxD mm Healthy
Observer 1	74	79	0.09	0.20	3.29	3.61
Observer 2	66	73	0.11	0.20	2.70	3.00
Observer 3	76	80	0.09	0.15	3.07	3.25
Wang et al. [13]	68	72	0.15	0.40	4.06	5.23
Shahzad et al. [14]	63	68	0.14	0.26	2.81	3.49
Proposed method	70	74	0.12	0.23	2.59	2.95

1. Dice = Dice similarity index, MSD = mean square distance, MaxD = Hausdorff distance, % = percentage, mm = millimeters (see the study of [29] for more details)

Table 5 The measurement values of the four metrics obtained by compared with the methods based on deep learning

Method	TP	FP	JM	DC
Gu et al. [17]	0.9221 ± 0.0411	0.1579 ± 0.1472	0.8101 ± 0.0940	0.9017 ± 0.0524
Shen et al. [18]	0.9396 ± 0.0371	0.1233 ± 0.1110	0.8378 ± 0.0818	0.9189 ± 0.0579
Proposed method	0.9697 ± 0.0370	0.0761 ± 0.0909	0.8912 ± 0.1021	0.9401 ± 0.0700

1. All data are presented in the form of mean ± standard deviation

Table 6 The computational cost of the critical procedures when applied to each data set (unit is seconds)

Metrics	The initial seed point	SRF	Local clustering segmentation	Total time	Cross-section based on HMT
Mean	2.2276	0.4887	0.5637	3.5420	18.6789
Std	0.5666	0.0971	0.1246	0.9377	7.4915

1. Std = Standard deviation.

imental results (see Table 5) showed that our method is better than theirs. Although the methods based on deep learning have been widely used in vessel segmentation and have achieved good results, coronary artery segmentation in coronary CTA images is still not well. Since the coronary arteries are small with various shapes and lesions, they can be affected by various kinds of noise and imaging factors. In addition, coronary artery segmentation based on deep learning needs numerous training data to have good adaptability and generalization. However, it is difficult for us to obtain numerous training data in practice, which can lead to poor results.

In terms of the computational cost, the average total time of the proposed method to process each of the 210 data sets was 3.5420 ± 0.9377 s, which can fully meet the clinical application.

The proposed method has achieved good results in coronary artery segmentation and can meet the clinical application. However, there are still two limitations.

1. The initialization of parameters. Although the proposed method with the various parameters adopted in this paper can segment the coronary artery, a fully automatic segmentation without any empirical parameters increases the reliability and robustness of the method for abnormal data. Hence, future studies will be conducted to seg-

ment coronary arteries effectively without any empirical parameters.

2. The initial seed points. Obtaining the initial seed points causes a high computational cost. Comparing the advantages and disadvantages of deep learning to the small number of data sets, we plan to combine the two methods in future work to reduce computing time and post-processing procedures.

Conclusion

In this study, a fully automatic method based on SRF and D-means local clustering for the segmentation of coronary CTA images is presented. The SRF is used to filter the vessel region to address the problem of segmentation caused by noise, artifacts, and non-coronary regions in the coronary CTA images. Furthermore, using the local clustering segmentation algorithm based on D-means can address the problem of large changes in CT values, dislocation of coronary arteries, and blurry artifacts in coronary CTA images, to quickly, stably, efficiently, and effectively segment the coronary artery. The experimental results of the quantitative analysis showed that the segmentation results of the proposed method are consistent with the three manual delineations within the error

range, which also fit abnormal data and can meet the clinical applications.

Acknowledgements This work was supported in part by National Natural Science Foundation of China (No. 61971118).

Declarations

Conflict of interest The authors declare that they have no conflict of interest.

Human and animal rights This article does not contain any studies with human participants or animals performed by any of the authors.

References

- Miller CL, Kontorovich AR, Hao K, Ma L, Iyegbe C, Björkegren JL, Kovacic JC (2021) Precision medicine approaches to vascular disease: Jacc focus seminar 2/5. *J Am Coll Cardiol* 77(20):2531–2550
- Sharim J, Budoff M (2021) Efficacy of coronary computed tomography angiography in assessing regression of coronary artery disease. *J Am Coll Cardiol* 77(18):1283
- Lesage D, Angelini ED, Bloch I, Funka-Lea G (2009) A review of 3d vessel lumen segmentation techniques: Models, features and extraction schemes. *Med Image Anal* 13(6):819–845
- Li S, Kong X, Lu C, Zhu J, He X, Fu R (2021) Gca-net: global context attention network for intestinal wall vascular segmentation. *Int J Comput Assist Radiol Surg* 1–10
- Boskamp T, Rinck D, Link F, Kummerlen B, Stamm G, Mildenerberger P (2004) New vessel analysis tool for morphometric quantification and visualization of vessels in ct and mr imaging data sets. *Radiographics* 24(1):287–297
- Huang X (2021) Intelligent algorithms-based ct image segmentation in patients with cardiovascular diseases and realization of visualization algorithms. *Sci Program*
- Jaquet C, Najman L, Talbot H, Grady L, Schaap M, Spain B, Kim HJ, Vignon-Clementel I, Taylor CA (2019) Generation of patient-specific cardiac vascular networks: a hybrid image-based and synthetic geometric model. *IEEE Trans Biomed Eng* 66(4):946–955
- Hammouche A, Cloutier G, Tardif JC, Hammouche K, Meunier J (2019) Automatic ivus lumen segmentation using a 3d adaptive helix model. *Comput Biol Med* 107:58–72
- Zhuang S, Li F, Raj ANJ, Ding W, Zhou W, Zhuang Z (2021) Automatic segmentation for ultrasound image of carotid intimal-media based on improved superpixel generation algorithm and fractal theory. *Comput Methods Programs Biomed* 205:106084
- Frangi AF, Niessen WJ, Vincken KL, Viergever MA (1998) Multiscale vessel enhancement filtering. In: *International conference on medical image computing and computer-assisted intervention*, Springer, pp 130–137
- Ge S, Shi Z, Peng G, Zhu Z (2019) Two-steps coronary artery segmentation algorithm based on improved level set model in combination with weighted shape-prior constraints. *J Med Syst* 43(7):1–10
- Gülsün MA, Tek H (2008) Robust vessel tree modeling. In: *International conference on medical image computing and computer-assisted intervention*. Springer, pp 602–611
- Wang C, Moreno R, Smedby Ö (2012) Vessel segmentation using implicit model-guided level sets. In: *MICCAI Workshop*3D cardiovascular imaging: a MICCAI segmentation Challenge**, Nice France, 1st of October 2012
- Shahzad R, van Walsum T, Kirisli H, Tang H, Metz C, Schaap M, van Vliet L, Niessen W (2012) Automatic stenoses detection, quantification and lumen segmentation of the coronary arteries using a two point centerline extraction scheme. In: *MICCAI 2012 workshop proceedings*
- Du H, Shao K, Bao F, Zhang Y, Gao C, Wu W, Zhang C (2021) Automated coronary artery tree segmentation in coronary cta using a multiobjective clustering and toroidal model-guided tracking method. *Comput Methods Programs Biomed* 199:105908
- Tan T, Wang Z, Du H, Xu J, Qiu B (2021) Lightweight pyramid network with spatial attention mechanism for accurate retinal vessel segmentation. *Int J Comput Assist Radiol Surg* 16(4):673–682
- Gu J, Fang Z, Gao Y, Tian F (2020) Segmentation of coronary arteries images using global feature embedded network with active contour loss. *Comput Med Imaging Graph* 86:101799
- Shen Y, Fang Z, Gao Y, Xiong N, Zhong C, Tang X (2019) Coronary arteries segmentation based on 3d fcn with attention gate and level set function. *IEEE Access* 7:42826–42835
- Abdelrahman KM, Chen MY, Dey AK, Virmani R, Finn AV, Khamis RY, Choi AD, Min JK, Williams MC, Buckler AJ (2020) Coronary computed tomography angiography from clinical uses to emerging technologies: Jacc state-of-the-art review. *J Am Coll Cardiol* 76(10):1226–1243
- Jodas DS, Pereira AS, Tavares JMR (2017) Automatic segmentation of the lumen region in intravascular images of the coronary artery. *Med Image Anal* 40:60–79
- Wiemker R, Klinder T, Berghtholdt M, Meetz K, Carlsen IC, Bülow T (2013) A radial structure tensor and its use for shape-encoding medical visualization of tubular and nodular structures. *IEEE Trans Visual Comput Graphics* 19(3):353–366
- Moreno R, Smedby Ö (2015) Gradient-based enhancement of tubular structures in medical images. *Med Image Anal* 26(1):19–29
- Xiao R, Yang J, Ai D, Fan J, Liu Y, Wang G, Wang Y (2015) Adaptive ridge point refinement for seeds detection in x-ray coronary angiogram. *Comput Math Methods Med*
- Sukanya A, Rajeswari R, Subramanian Murugan K (2020) Region based coronary artery segmentation using modified frangi's vesselness measure. *Int J Imaging Syst Technol* 30(3):716–730
- Dubey AK, Gupta U, Jain S (2016) Analysis of k-means clustering approach on the breast cancer wisconsin dataset. *Int J Comput Assist Radiol Surg* 11(11):2033–2047
- Yu X, Zhai J, Zou B, Shao Q, Hou G (2021) A novel acoustic sediment classification method based on the k-mdoids algorithm using multibeam echosounder backscatter intensity. *J Mar Sci Eng* 9(5):508
- Jang HJ, Kim B (2021) Km-dbscan: density-based clustering of massive spatial data with keywords. *Human Centric Comput Inf Sci* 11
- Lin Y, Chen S (2021) A centroid auto-fused hierarchical fuzzy c-means clustering. *IEEE Trans Fuzzy Syst* 29(7):2006–2017
- Kirişli H, Schaap M, Metz C, Dharampal A, Meijboom WB, Papadopoulou SL, Dedic A, Nieman K, de Graaf MA, Meijjs M (2013) Standardized evaluation framework for evaluating coronary artery stenosis detection, stenosis quantification and lumen segmentation algorithms in computed tomography angiography. *Med Image Anal* 17(8):859–876

Publisher's Note Springer Nature remains neutral with regard to jurisdictional claims in published maps and institutional affiliations.